J. Fluid Mech. (1995), *vol.* 289, *pp.* 243–261

The motion of axisymmetric dipolar particles in homogeneous shear flow

By Y. ALMOG[1]† AND I. FRANKEL[2]

[1] Faculty of Mathematics, Technion – Israel Institute of Technology, Haifa 32000, Israel

[2] Faculty of Aerospace Engineering, Technion – Israel Institute of Technology, Haifa 32000, Israel

(Received 16 July 1993 and in revised form 26 Oct. 1994)

The respective effects of an external field and departure of suspended particles from spherical shape on the rotary motion of axisymmetric dipolar particles placed in a homogeneous shear flow are studied. The analysis shows that, owing to cumulative effects, even a weak external field or a small deviation from spherical shape can significantly modify the resulting motion relative to that found in the corresponding classical problems of torque-free particles or dipolar spheres in homogeneous shear. Thus, unlike the latter problems, there are in the present problem cases when all particles approach a single limit cycle; in other cases multiple stable equilibria simultaneously coexist and the orientation space is appropriately divided into corresponding domains of attraction; in some situations possessing appropriate symmetry properties, particles may, depending upon their respective initial orientations, either move along a family of periodic orbits or else converge to a stable equilibrium orientation.

1. Introduction

We study the rotary motion of a non-spherical dipolar particle placed in a (macroscopically) homogeneous shear flow in the presence of an external field. This motion is essentially governed by a pair of competing orienting mechanisms: (i) the shear field which, depending on particle shape and the relative magnitude of the strain and rotation (the respective symmetric and antisymmetric) components of the undisturbed fluid-velocity gradient, tends to align the non-spherical particle with the principal directions of strain or else rotate it about the fluid vorticity vector; (ii) the orienting torque acting to align the embedded dipole with the external field. Such interaction with an external field may result for instance from asymmetry of particle superficial geometry or internal mass distribution (e.g. an asymmetric dumbbell under gravity) as well as from magnetic or other material properties (e.g. a ferromagnetic particle in the presence of a magnetic field).

Apart from the fundamental interest in the present problem, the subsequent analysis is relevant to the macroscopic description of the transport phenomena and rheological properties of (dilute) suspensions of such non-spherical dipolar particles (e.g. the potential of controlling the rheological behaviour of a ferrofluid by means of an appropriate external magnetic field).

The rotary motion in a simple shear flow of spheroids was first analysed by Jeffery (1922). In the absence of external torques it was possible to integrate the equations of

† Present address: Department of Mathematics, Massachusetts Institute of Technology, Cambridge MA 02139, USA.

motion to obtain closed-form analytical expressions for the periodic particle orbits. The analysis was later extended by Bretherton (1962) to general axisymmetric particles possessing fore-aft symmetry and by Hinch & Leal (1979) who investigated the motion of triaxial ellipsoids.

The incorporation into the problem of the additional element of external torques considerably complicates the analysis. Thus, even for spherical particles, integration of the equations of motion is only possible in the particular cases when the external field is either parallel or perpendicular to the fluid vorticity vector. This latter problem, of spherical dipolar particles, was first discussed by Hall & Busenberg (1969).

Following the formulation in the next section of the general problem for the rotary motion of an axisymmetric dipolar particle, we present a phase-plane analysis of the particular cases when the external field is either perpendicular (§3) or parallel (§4) to the plane of the (simple) shear flow. In §5 we make use of some asymptotic results and provide a qualitative picture of particle motion when the external field acts in an arbitrary direction. Concluding remarks summarizing the main results of the present contribution appear in §6.

2. Formulation of the problem

Consider an axisymmetric dipolar particle placed in a homogeneous shear flow under the action of an external field. The orientation of the particle can be represented by the unit vector $\boldsymbol{e}$ attached to its axis of symmetry (figure 1), thus its motion in orientation space may be described by an appropriate trajectory on S_2, the surface of the unit sphere. Assuming that the particle Reynolds number is small and neglecting the effects of particle and fluid inertia, $\boldsymbol{e}$ satisfies the equations of motion

$$\dot{\boldsymbol{e}} = (\boldsymbol{\omega}_f - \boldsymbol{B}:\boldsymbol{S} + m_r \boldsymbol{T}) \times \boldsymbol{e}, \tag{2.1}$$

wherein $\dot{\boldsymbol{e}}$ denotes the time derivative of $\boldsymbol{e}$, $\boldsymbol{\omega}_f$ is the angular velocity of the fluid and $\boldsymbol{S}$ is the rate of strain – the symmetric part of the (undisturbed) fluid-velocity gradient. The third-order pseudotensor $\boldsymbol{B} = \boldsymbol{B}(\boldsymbol{e})$ is the orientation-specific shear-diffusion coefficient. For a body of revolution $\boldsymbol{B}$ is expressible in the form

$$\boldsymbol{B} = \tfrac{1}{2}B[\boldsymbol{\varepsilon}\cdot\boldsymbol{ee} + (\boldsymbol{\varepsilon}\cdot\boldsymbol{ee})^{\dagger}] \tag{2.2a}$$

in which $\boldsymbol{\varepsilon}$ is the permutation pseudotensor, and for a third-order tensor the post-transposition operator denotes $(A_{ijk})^{\dagger} = A_{ikj}$. The scalar B is an intrinsic coefficient; for a spheroid whose axis ratio is R

$$B = \frac{R^2 - 1}{R^2 + 1} \tag{2.2b}$$

and thus obviously $|B| < 1$. (For axisymmetric particles of arbitrary shape R represents an effective axis ration.) Finally, m_r is the mobility coefficient corresponding to rotation of the particle about a transverse axis and $\boldsymbol{T}$ is the torque exerted on the particle by the (presumably constant) external field $\boldsymbol{F}$

$$\boldsymbol{T} = \boldsymbol{M} \times \boldsymbol{F}, \tag{2.3}$$

where $\boldsymbol{M} = \mu \boldsymbol{e}$ is the (permanent) dipole moment of the particle.

The present analysis focuses on the simple shear flow

$$\boldsymbol{u} = \hat{\boldsymbol{j}} G x, \tag{2.4}$$

wherein $(\hat{\boldsymbol{i}}, \hat{\boldsymbol{j}}, \hat{\boldsymbol{k}})$ is a right-handed triad of orthonormal space-fixed unit vectors in the

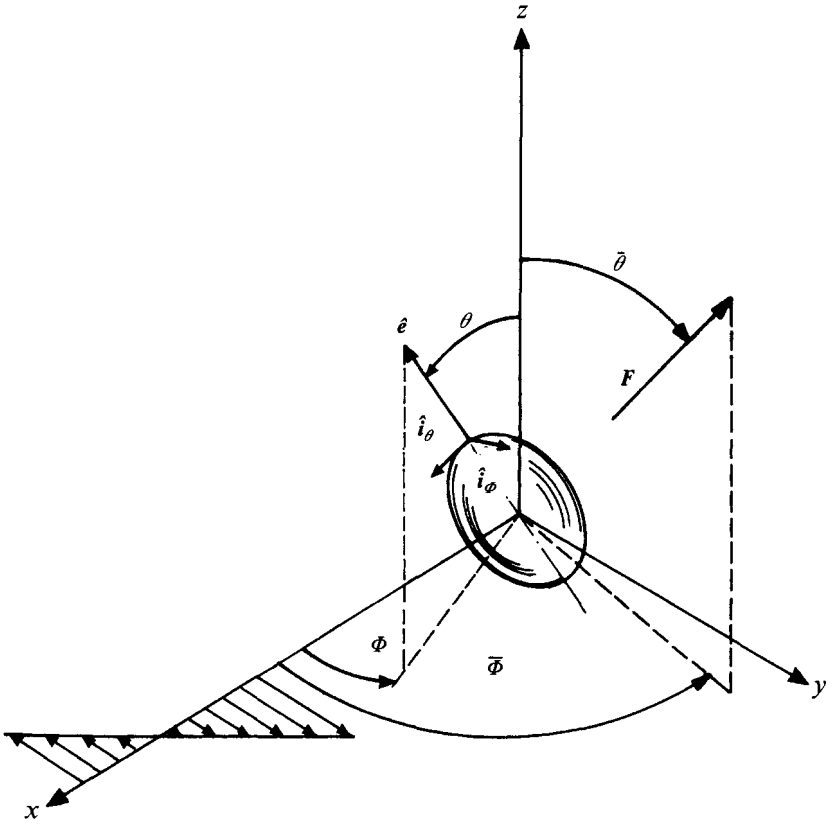

FIGURE 1. Definition of axisymmetric particle orientation $\boldsymbol{e} \equiv (\theta, \phi)$ in a simple shear flow.

directions of the (x, y, z) axes, respectively, and the scalar G denotes the rate of shear. It is, however, worthwhile to mention that (cf. Bretherton 1962; Hinch & Leal 1972*a*; Brenner 1974) through an appropriate reinterpretation of the above parameters B and G, the applicability of subsequent results can be extended readily to the wider class of planar homogeneous shear flows

$$\boldsymbol{u} = \hat{\boldsymbol{i}}(E-\Omega)\, y + \hat{\boldsymbol{j}}(E+\Omega)\, x \tag{2.5a}$$

provided that

$$BE < \Omega. \tag{2.5b}$$

In the foregoing E and Ω are, respectively, the magnitudes of the rate of strain and (half) the vorticity in the flow field $\boldsymbol{u}$. The latter restriction thus ensures that the influence of the fluid vorticity acting to rotate the particle prevails over the tendency to align its axis with one of the principal direction of $\boldsymbol{S}$, thus leading, in the absence of an external field, to a periodic rotary motion of the particle characterized by closed orbits on S_2. When (2.5*b*) is not satisfied as, for instance, when a particle for which $|B| > 1$ is placed in a simple shear flow ($E = \Omega$), the foregoing balance is reversed and the motion is qualitatively different (Bretherton 1962). In subsequent analysis we assume that $|B| < 1$.

Let $(\boldsymbol{e}, \hat{\boldsymbol{i}}_\theta, \boldsymbol{i}_\phi)$ be a right-handed triad of particle-fixed unit vectors and (θ, ϕ) spherical polar coordinates (figure 1). Expressing $\dot{\boldsymbol{e}}$ in this frame of reference,

$$\dot{\boldsymbol{e}} = \hat{\boldsymbol{i}}_\theta \dot{\theta} + \hat{\boldsymbol{i}}_\phi \dot{\phi} \sin\theta, \tag{2.6}$$

one obtains from (2.1) a pair of coupled autonomous first-order scalar equations for θ and ϕ as functions of the non-dimensional time $\tau = Gt$:

$$\dot{\phi} = \tfrac{1}{2}(1 + B\cos 2\phi) - \lambda \frac{\sin\bar{\theta}}{\sin\theta}\sin(\phi - \bar{\phi}), \tag{2.7a}$$

and

$$\dot{\theta} = \tfrac{1}{4}B\sin 2\theta \sin 2\phi + \lambda[\sin\bar{\theta}\cos\theta\cos(\phi - \bar{\phi}) - \cos\bar{\theta}\sin\theta]. \tag{2.7b}$$

In the above the polar angles $(\bar{\theta}, \bar{\phi})$ represent the direction of the external field (cf. figure 1) and the dimensionless parameter $\lambda = \mu m_r F/G$ (in which $F = |\boldsymbol{F}|$) represents the relative effects on the particle rotation of the external field and the fluid shear, respectively. In the respective limits $\lambda = 0$ and $B = 0$ the latter equations reduce to the classical problems of the motion in simple shear of torque-free axisymmetric particles and dipolar spheres. The rest of this contribution examines the respective effects of the external field and departure from spherical shape on the motion of a dipolar particle.

It is useful to note that the problem posed by (2.7) remains invariant under the following transformations:

(i) $$\bar{\theta} \to \pi - \bar{\theta}, \quad \theta \to \pi - \theta; \tag{2.8a}$$

(ii) $$\bar{\phi} \to \bar{\phi} + \pi, \quad \phi \to \phi + \pi; \tag{2.8b}$$

and

(iii) $$B \to -B, \quad \bar{\phi} \to \bar{\phi} + \tfrac{1}{2}\pi, \quad \phi \to \phi + \tfrac{1}{2}\pi. \tag{2.8c}$$

These symmetry properties respectively allow us to make the following restrictions: (i) $\bar{\theta}$ to the interval $[0, \frac{1}{2}\pi]$, and (ii) $\bar{\phi}$ to the interval $[0, \pi]$,, as well as (iii) consider only prolate particles $0 \leqslant B < 1$, without loss of generality. For later reference we mention the additional invariance under the transformation

(iv) $$\bar{\theta} \to \pi - \bar{\theta}, \quad \bar{\phi} \to \pi - \bar{\phi}, \quad \phi \to -\phi, \quad \tau \to -\tau. \tag{2.8d}$$

Thus, when the direction of the external field is reflected with respect to the direction to fluid velocity ($\hat{\boldsymbol{j}}$), the corresponding particle trajectories are obtained through reflection with respect to the (x, z)-plane and, a reversal of the sense of the motion along the resulting paths.

3. External field acting perpendicularly to the plane of flow ($\bar{\theta} = 0$)

When $\bar{\theta} = 0$ the system (2.7) reduces to

$$\dot{\phi} = \tfrac{1}{2}(1 + B\cos 2\phi) \tag{3.1a}$$

and

$$\dot{\theta} = \tfrac{1}{4}B\sin 2\theta \sin 2\phi - \lambda \sin\theta. \tag{3.1b}$$

The first of these equations is identical to the corresponding equation governing the rotary motion of an axisymmetric particle in the absence of an external field and is thus readily integrated to yield the classical result for $\phi(\tau)$ (see (5.4a), (5.5a)). When $|B| < 1$, $\dot{\phi} > 0$ for all $(\theta, \phi) \in S_2$. Thus, ϕ grows monotonically which means that $\boldsymbol{e}$ rotates about the vorticity vector. From (3.1b) we see that when the external torque is sufficiently strong, namely $\lambda > B/2$, $\dot{\theta} < 0$ over the entire S_2 domain (excluding the poles $\theta = 0, \pi$), in which case all the trajectories, except for the one starting at the unstable equilibrium point $\theta = \pi$, monotonically converge to the stable equilibrium point $\theta = 0$. If $\lambda < B/2$ there exist domains in S_2 where $\dot{\theta} > 0$. However, even in this

case, for any initial condition ($\theta_0 \neq \pi$), $\lim_{\tau\to\infty}\theta(\tau) = 0$, although the convergence is not necessarily monotonical. This latter statement is readily verified by comparison with the case $\lambda = 0$. Starting at some arbitrary point (θ_0, ϕ_0) in S_2, the Jeffery orbit returns after an entire period of 2π in ϕ to the same point. Evidently, from (3.1*b*) $\mathrm{d}\theta/\mathrm{d}\phi|_{\lambda>0} < \mathrm{d}\theta/\mathrm{d}\phi|_{\lambda=0}$, hence no orbit representing a solution of (3.1) can possibly intersect the Jeffery orbit corresponding to the same initial condition (ϕ_0, ϕ_0). Therefore, $\theta(\phi_0) > \theta(\phi_0+2\pi)$ and the sequence $\{\theta(\phi_0+2\pi n)\}_{n=0}^{\infty}$ is monotonically decreasing and hence converges to the only possible limit, namely $\theta = 0$. It can be established† that under the action of a strong ($\lambda \gg 1$) external field, $\theta(\tau)$ is approximated (for all τ) by

$$\tan\tfrac{1}{2}\theta \approx \tan\tfrac{1}{2}\theta(0)\,(1+B\cos 2\phi)^{-1/2}[1+O(\lambda^{-1})]\,\mathrm{e}^{-\lambda\tau}. \tag{3.2}$$

A similar exponentially rapid convergence to the stable equilibrium orientation is also expected in the presence of an arbitrarily oriented ($\bar{\theta} \neq 0$) strong ($\lambda \gg 1$) external field. The other limit ($\lambda \ll 1$) is considered in §5 within the broader context of arbitrarily directed weak external fields. The analysis shows that, when $\lambda \ll 1$, the particle slowly drifts across Jeffery's orbits, gradually spiralling towards $\theta = 0$.

4. External field acting in the plane of shear ($\bar{\theta} = \frac{1}{2}\pi$)

In this case we obtain from (2.7)

$$\dot{\phi} = \tfrac{1}{2}(1+B\cos 2\phi) - \lambda\frac{\sin(\phi-\bar{\phi})}{\sin\theta} \tag{4.1a}$$

and

$$\dot{\theta} = \tfrac{1}{4}B\sin 2\theta\sin 2\phi + \lambda\cos\theta\cos(\phi-\bar{\phi}). \tag{4.1b}$$

Here particle trajectories are symmetric relative to the equator $\theta = \frac{1}{2}\pi$ (cf. (2.8*a*)). We therefore limit subsequent analysis to the upper hemispherical domain $0 \leqslant \theta \leqslant \frac{1}{2}\pi$.

4.1. *The lines* $\dot{\phi} = 0$, $\dot{\theta} = 0$

From (4.1*a*), $\dot{\phi} = 0$ when

$$\sin\theta = \frac{2\lambda\sin(\phi-\bar{\phi})}{1+B\cos 2\phi}. \tag{4.2}$$

Since $\sin\theta \geqslant 0$ throughout S_2, the curves $\dot{\phi} = 0$ only exist in the domain $0 \leqslant \phi-\bar{\phi} \leqslant \pi$ and pass through the pole $\theta = 0$ in the directions $\phi = \bar{\phi}$, $\phi = \bar{\phi}+\pi$. Transformation of (4.2) into Cartesian coordinates reveals that the projection of the curve $\dot{\phi} = 0$ onto the shear (x,y)-plane is an ellipse whose axes are respectively parallel to the (x,y) coordinate axes. For sufficiently small $\lambda < \lambda_1 = (1-B)/2$, this ellipse is contained within the domain $0 \leqslant \theta < \sin^{-1}(\lambda/\lambda_1)$ (cf. the dash-dotted line in figure 3*b*). When $\lambda > \lambda_2 = (1+B)/2$ the ellipse $\dot{\phi} = 0$ necessarily intersects the unit circle (the 'equator'). In general, the points of intersection are obtained from the solution of a quartic algebraic equation. When λ is sufficiently large there always exist two intersections (e.g. the points A and C in figure 3*a*) which, in the limit $\lambda\to\infty$, approach the respective directions $\bar{\phi}$ and $\bar{\phi}+\pi$. Finally, for sufficiently large $|B|$ (i.e. particles significantly deviating from a spherical shape) and $\bar{\phi}$ sufficiently close to $\frac{1}{2}\pi$ (i.e. a sufficiently small angle between the respective directions of the external field and the undisturbed streamlines), there exists an intermediate domain of λ values where four intersection points appear (cf. points A, B, C and D in figure 5).

† Details of the calculation may be obtained upon request directly from the authors or from the *Journal of Fluid Mechanics* Editorial Office.

From (4.1*b*), the requirement $\dot{\theta} = 0$ is satisfied on the equator, $\theta = \frac{1}{2}\pi$, as well as when

$$\sin\theta = -\frac{2\lambda\cos(\phi-\bar{\phi})}{B\sin 2\phi}. \tag{4.3}$$

Since the solutions of (4.3) satisfy $\theta(\phi+\frac{1}{2}\pi, \bar{\phi}-\frac{1}{2}\pi, B) = \theta(\phi, \bar{\phi}, B)$, the discussion can be confined to the domain $0 \leqslant \bar{\phi} \leqslant \frac{1}{2}\pi$. The transformation of (4.3) into Cartesian coordinates shows that the projection of the curve $\dot{\theta} = 0$ onto the (x, y)-plane is a hyperbola whose asymptotes are, respectively, parallel to the coordinate axes. The branch of this hyperbola which passes through the pole $\theta = 0$ in the direction $\phi = \bar{\phi} \pm \frac{1}{2}\pi$ is always physically meaningful (cf. the dashed curve BOD in figure 3). The second branch only appears within the unit circle for sufficiently small $\lambda(< |B|[(\cos\bar{\phi})^{2/3} + (\sin\bar{\phi})^{2/3}]^{3/2})$. Finally, in the cases $\bar{\phi} = 0, \frac{1}{2}\pi$ the lines $\dot{\theta} = 0$ either coincide with or are parallel to the (x, y)-axes (cf. figure 5*b*).

4.2. *Equilibrium (critical) points*

The above examination of the lines $\dot{\phi} = 0$ and $\dot{\theta} = 0$ indicates the possible existence of two kinds of equilibrium points:

(i) points on the equator ($\theta = \frac{1}{2}\pi$), which exist provided that the ellipse $\dot{\phi} = 0$ intersects with the equator;

(ii) points off the equator, at which (4.2) and (4.3) are simultaneously satisfied by

$$\tan\phi_c = -R^2\cot\bar{\phi}, \tag{4.4a}$$

$$\sin\theta_c = \frac{2\lambda}{1+B}(R^4\cos^2\bar{\phi} + \sin^2\bar{\phi})^{1/2}. \tag{4.4b}$$

From these expressions, it is evident that such points do not exist for $\lambda > \lambda_2$ whereas for $\lambda < \lambda_1$ they exist irrespective of the value of $\bar{\phi}$.

The nature of the equilibrium (critical) points $\boldsymbol{e}_c = (\theta_c, \phi_c)$ is examined by making reference to the Liapunov theorem relating in the present problem their stability to the eigenvalues of the (two-dimensional) surface dyadic†

$$\boldsymbol{\nabla}_e \dot{\boldsymbol{e}}|_{e_c} = \hat{\boldsymbol{i}}_\theta\hat{\boldsymbol{i}}_\theta\frac{\partial\dot{\theta}}{\partial\theta} + \hat{\boldsymbol{i}}_\theta\hat{\boldsymbol{i}}_\phi\frac{\partial}{\partial\theta}(\dot{\phi}\sin\theta) + \hat{\boldsymbol{i}}_\phi\hat{\boldsymbol{i}}_\theta\frac{1}{\sin\theta}\frac{\partial\dot{\theta}}{\partial\phi} + \hat{\boldsymbol{i}}_\phi\hat{\boldsymbol{i}}_\phi\frac{\partial\dot{\phi}}{\partial\phi}. \tag{4.5}$$

Thus, according to the latter theorem, the existence of an eigenvalue possessing a positive real part is a sufficient condition for instability. However, if all the eigenvalues of $\boldsymbol{\nabla}_e \dot{\boldsymbol{e}}|_{e_c}$ have negative real parts, the equilibrium point is stable. At an equilibrium point on the equator ($\theta_c = \frac{1}{2}\pi$)

$$\boldsymbol{\nabla}_e \dot{\boldsymbol{e}}|_{e_c} = -\hat{\boldsymbol{i}}_\theta\hat{\boldsymbol{i}}_\theta[\lambda\cos(\phi_c-\bar{\phi}) + \tfrac{1}{2}B\sin 2\phi_c] - \hat{\boldsymbol{i}}_\phi\hat{\boldsymbol{i}}_\phi[\lambda\cos(\phi_c-\bar{\phi}) + B\sin 2\phi_c]. \tag{4.6}$$

The scalar coefficient of $\hat{\boldsymbol{i}}_\phi\hat{\boldsymbol{i}}_\phi$ is $(\partial\dot{\phi}/\partial\phi)_{\theta=\pi/2}$ (see (4.5) and (4.1*a*)). Since $\dot{\phi}$ is a periodic function of ϕ, half of the equilibrium points (where $\dot{\phi}$ is an increasing function of ϕ) are unstable and the other half (where $\dot{\phi}$ is decreasing) are stable with regard to

† The rotary motion of the particles can be represented by the three-dimensional velocity field $\boldsymbol{v} = r\boldsymbol{e}$ corresponding to translational motion of the particles on spherical ($r = \text{const}$) surfaces. At the point $\boldsymbol{r} = r\boldsymbol{e}$, the velocity gradient is the three-dimensional dyadic $\boldsymbol{\nabla v} = \boldsymbol{e}\dot{\boldsymbol{e}} + \boldsymbol{\nabla}_e\dot{\boldsymbol{e}}$ wherein $\boldsymbol{\nabla}_e = \hat{\boldsymbol{i}}_\theta\partial/\partial\theta + \hat{\boldsymbol{i}}_\phi(1/\sin\theta)\,\partial/\partial\phi$ is the surface portion of the three-dimensional gradient operator. At a critical point, however, the first term in the expression for $\boldsymbol{\nabla v}$ vanishes and the second term reduces to the two-dimensional dyadic (4.5).

disturbances in the $\hat{\boldsymbol{i}}_\phi$ direction. The scalar coefficient of $\hat{\boldsymbol{i}}_\theta \hat{\boldsymbol{i}}_\theta$ is $(\partial\dot{\theta}/\partial\theta)_{\theta=\pi/2}$ (see (4.5) and (4.1*b*)). Thus, if for $\theta < \frac{1}{2}\pi$ ($\theta > \frac{1}{2}\pi$) we have $\dot{\theta} > 0$ ($\theta < 0$), then this coefficient is negative and the equilibrium point is accordingly stable to disturbances in the $\hat{\boldsymbol{i}}_\theta$ direction and vice versa.

At an equilibrium point $\boldsymbol{e} = \boldsymbol{e}_c$ off the equator, we obtain from (4.2) in conjunction with (4.3)

$$\nabla_{\boldsymbol{e}} \dot{\boldsymbol{e}}|_{\boldsymbol{e}_c} = \tfrac{1}{2}\hat{\boldsymbol{i}}_\theta \hat{\boldsymbol{i}}_\theta B \sin 2\phi_c \cos^2\theta_c - \tfrac{1}{2}\hat{\boldsymbol{i}}_\phi \hat{\boldsymbol{i}}_\theta (1 - B\cos 2\phi_c)\cos\theta_c + \tfrac{1}{2}\hat{\boldsymbol{i}}_\theta \hat{\boldsymbol{i}}_\phi (1 + B\cos 2\phi_c)\cos\theta_c - \tfrac{1}{2}\hat{\boldsymbol{i}}_\phi \hat{\boldsymbol{i}}_\phi B \sin 2\phi_c. \quad (4.7)$$

Here, the eigenvalues of $\nabla_{\boldsymbol{e}} \dot{\boldsymbol{e}}|_{\boldsymbol{e}_c}$, $S_j (j = 1, 2)$, satisfy the quadratic equation

$$S_j^2 + (\tfrac{1}{2}B \sin^2\theta_c \sin 2\phi_c) S_j + \tfrac{1}{4}(1 - B^2)\cos^2\theta_c = 0. \quad (4.8)$$

Thus (cf. (4.4*a*)), $\boldsymbol{e}_c$ is a stable or an unstable critical point according to whether $\frac{1}{2}\pi < \bar{\phi} < \pi$ or $0 < \bar{\phi} < \frac{1}{2}\pi$, respectively. Furthermore, with increasing λ when $\boldsymbol{e}_c$ approaches the equator (cf. (4.4*b*)), the critical point which for small λ was a (stable or an unstable) spiral point, turns into a node (of the corresponding nature). Finally, when $\bar{\phi} = 0, \frac{1}{2}\pi$, the eigenvalues of $\nabla_{\boldsymbol{e}} \dot{\boldsymbol{e}}|_{\boldsymbol{e}_c}$ are purely imaginary which suggests that $\boldsymbol{e}_c$ may be either a centre or a spiral point. By invoking symmetry considerations, it will be established in the next subsection that all the solutions are periodic for $\bar{\phi} = 0, \frac{1}{2}\pi$ in which cases the equilibrium point $\boldsymbol{e}_c$ is indeed a centre.

The evolution with λ of the phase-plane configuration is summarized in figure 2 which describes the variation of the type and location of the (projections on the (x, y)-plane of the) critical points in the upper hemispherical domain for (*a*) $B = 0.5$, $\bar{\phi} = 45°$; and (*b*) $B = 0.8$, $\bar{\phi} = 88°$. The numbers on the figure indicate the corresponding values of λ. In both parts of the figure there initially appears, for small values of λ, only a single critical point. With increasing λ these points move away from $\theta = 0$ along straight radial lines (cf. (4.4*a*)).

In figure 2(*a*) these critical points are initially unstable spiral points marked by the crossed circles (this situation corresponds to the case presented in figure 3*b*). For $\lambda > 0.310$ these points turn into unstable nodes denoted by squares. At $\lambda = 0.323$ there appears the saddle-node point marked by the asterisk at the point where the ellipse $\dot{\phi} = 0$ first touches the unit circle. For each λ in the intermediate interval $0.323 < \lambda < 0.335$ following this saddle-node bifurcation there exist three critical points, namely a stable node and a saddle point on the equator (respectively denoted by the rhombi and triangles) together with an unstable node within the unit circle. At $\lambda = 0.335$ there appears another saddle-node bifurcation (marked by the asterisk at the common intersection of the ellipse $\dot{\phi} = 0$, the hyperbola $\dot{\theta} = 0$, and the unit circle). For still larger values of λ the saddle points disappear. There only remain the stable and unstable nodes on the equator (as in figure 3*a*). With increasing λ the former node approaches the direction $\bar{\phi}$ of the external field.

Figure 2(*b*) illustrates some qualitatively new features. Following the second bifurcation when, at $\lambda = 0.620$, the ellipse $\dot{\phi} = 0$ touches for the first time the lower part of the unit circle at the point marked by the corresponding asterisk, there appears the intermediate regime of λ values where four critical points simultaneously exist along the equator. For $0.620 < \lambda < 0.859$ these include a stable node, a pair of saddle points, and an unstable node (together with an unstable node or spiral point off the equator; see e.g. figure 5*a*). For $0.859 < \lambda < 0.901$, following the saddle-node bifurcation at $\lambda = 0.859$, there remain the four critical points on the unit circle (a pair of unstable nodes, a stable node and a saddle).

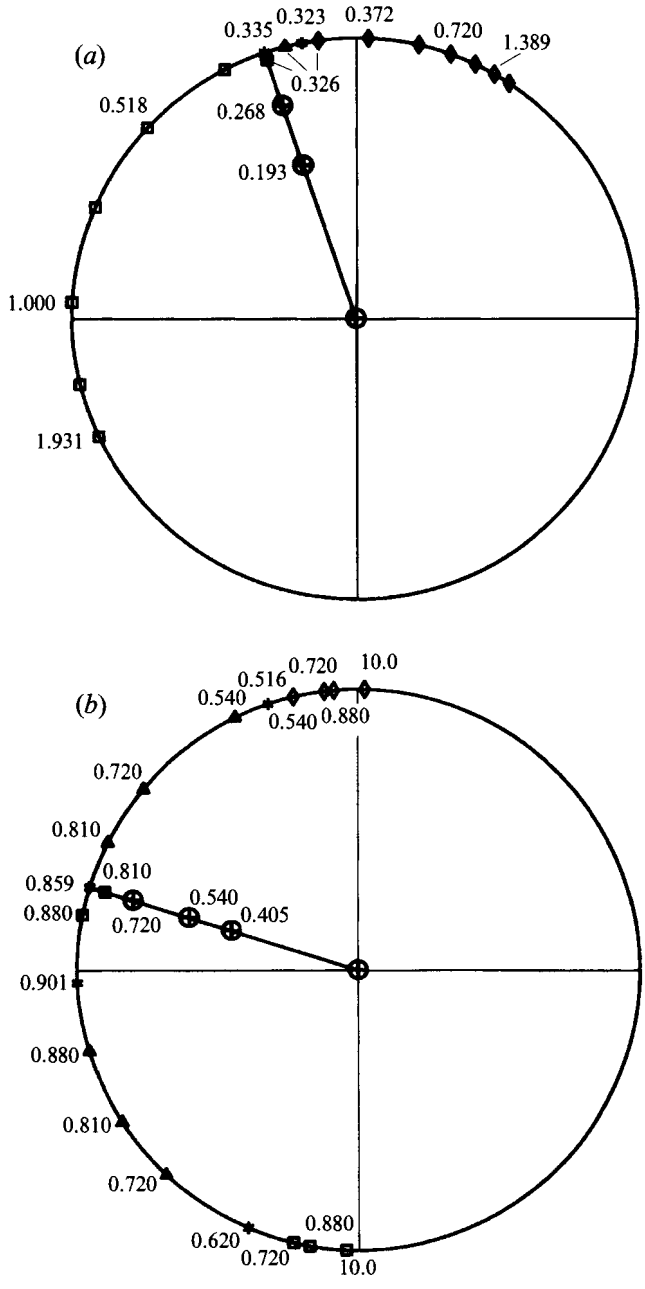

FIGURE 2. Variation of the location and nature of equilibrium points with the external field intensity λ, for (*a*) $\bar{\phi} = 45°$ and $B = 0.5$; (*b*) $\bar{\phi} = 88°$ and $B = 0.8$, $\diamond$, Stable node; $\square$, unstable node; $\oplus$, (unstable) spiral point; $\triangle$, saddle point; $*$, saddle node. The numbers indicate the corresponding values of λ.

In the case $\bar{\phi} = 90°$ (which is not presented here) the picture becomes symmetric with respect to the x-axis, the negative part of which is the locus of the critical points within the interior of the unit circle. It will be established later on that these points are centres (rather than spiral points, see figure 5*b*).

Making use of the symmetry property (2.8*d*) the description appropriate to

$90° < \bar{\phi} < 180°$ is obtainable via a reflection of the picture corresponding to $180° - \bar{\phi}$ with respect to the x-axis. The nature of the critical points thus obtained changes from stable to unstable and vice versa (cf. the discussion pertaining to figure 5*a*).

4.3. *Particle trajectories*

The results of the preceding subsections are now applied to obtain a qualitative description of particle paths in orientation space. We consider the cases where only a single branch of the hyperbola $\dot{\theta} = 0$ (namely, the one passing through the pole $\phi = 0$) is physically meaningful, while the ellipse corresponding to $\dot{\phi} = 0$ either intersects the equator twice or else is entirely enclosed within the unit circle. (The same approach could be applied to the analysis of all other cases.)

A typical description of the former case is presented in figure 3(*a*). The curves AOC and BOD, along which $\dot{\phi} = 0$ and $\dot{\theta} = 0$, respectively, divide the phase plane into the four domains marked by I, II, III and IV. The respective combinations of signs of $\dot{\phi}$ and $\dot{\theta}$ pertaining to the various domains are

$$\text{I}\{\dot{\theta} > 0,\ \dot{\phi} < 0\}, \quad \text{II}\{\dot{\theta} < 0,\ \dot{\phi} < 0\}, \tag{4.9a,b}$$

$$\text{III}\{\dot{\theta} < 0,\ \dot{\phi} > 0\}, \quad \text{IV}\{\dot{\theta} > 0,\ \dot{\phi} > 0\}. \tag{4.9c,d}$$

The short arrows marked on AOC and BOD point in the sense of admissible transitions between adjacent domains, namely

$$\text{III} \to \text{II}, \quad \text{III} \to \text{IV}, \quad \text{II} \to \text{I}, \quad \text{and} \quad \text{I} \to \text{IV}. \tag{4.10}$$

These are established by determining the signs of the respective second-order time derivatives $\ddot{\theta}|_{\dot{\theta}=0}$ and $\ddot{\phi}|_{\dot{\phi}=0}$. (Alternatively one can make use of (2.7) and (4.9) together with the convexity of both AOC and BOD.)

The above discussion enables the qualitative construction of particle trajectories (which are illustrated in the figure by the curves respectively originating at E_1 and E_2, obtained by numerical integration of (4.1)). A trajectory starting in region IV will stay there and therefore, since $\theta(\tau)$ and $\phi(\tau)$ are both monotonically increasing functions of τ, will eventually converge to the stable equilibrium point C. An orbit originating in I can converge to C either directly or via domain IV. A solution beginning in II must reach I and then C. Finally, a path starting at III must reach C, either exclusively through IV (like the one beginning at E_1), or via II, then I, and, possibly, IV (as in the trajectory starting at E_2). In summary, all possible trajectories eventually converge to the stable equilibrium at C. (This convergence to the stable equilibrium orientation can also be established from the Poincaré–Bendixon theorem since the absence of critical points within the interior of the unit circle excludes the possibility of periodic solutions in the present case.)

A typical phase-plane description of the second case to be considered appears in figure 3(*b*). As in the preceding figure, the curves $\dot{\phi} = 0$ and $\dot{\theta} = 0$, denoted respectively by the dash-dotted and dashed lines, divide the phase plane into the four domains – I, II, III and IV – at which $\dot{\phi}$, $\dot{\theta}$ satisfy the respective relations (4.9*a–d*). The admissible transitions between adjacent domains are established in a similar manner to the preceding example and are indicated by the respective short arrows on the curves $\dot{\phi} = 0$ and $\dot{\theta} = 0$. As a result we conclude that particle paths consist of either 'short'

$$\text{I} \to \text{II} \to \text{III} \to \text{IV} \to \text{I} \tag{4.11a}$$

(like the one starting near A) or 'long'

$$\text{I} \to \text{II} \to \text{I} \tag{4.11b}$$

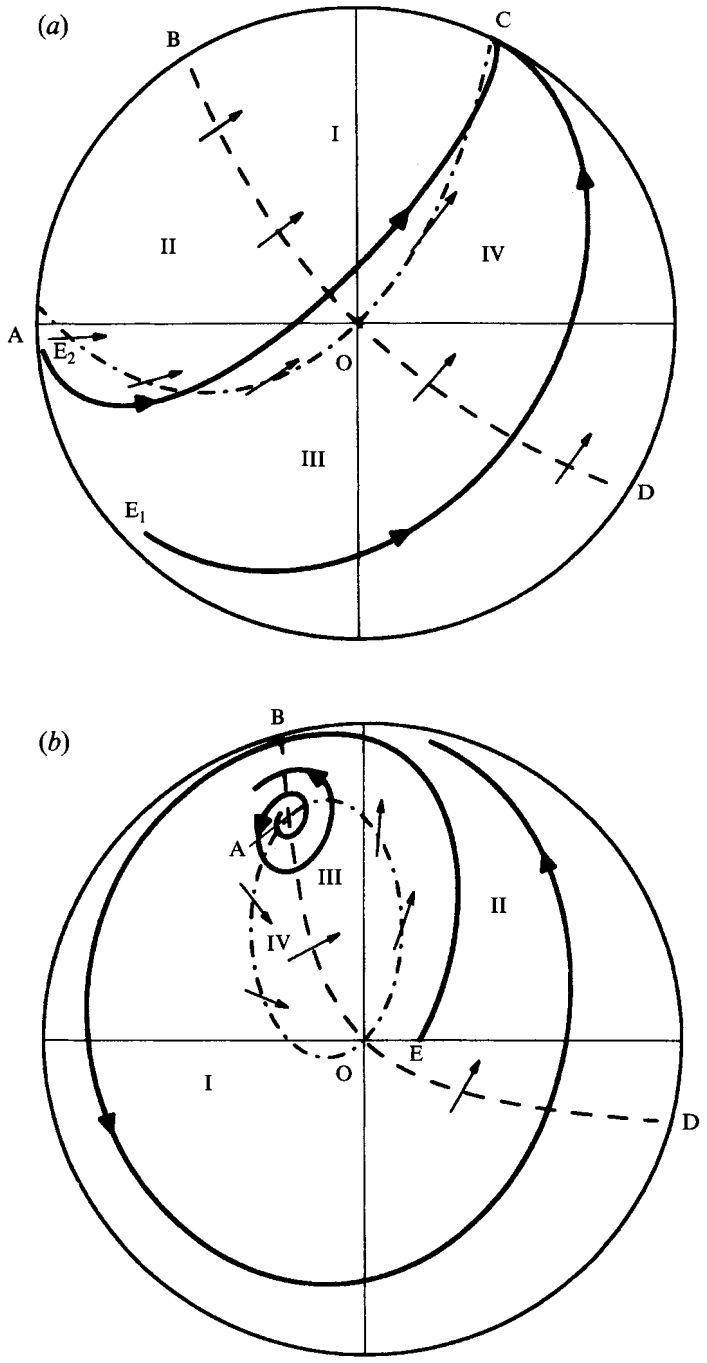

FIGURE 3. Projections on the plane of shear of particle trajectories in the case of an external field acting in the direction $\bar{\phi} = \frac{1}{4}\pi$ within the shear plane for $B = 0.5$ and (*a*) $\lambda = 1$, (*b*) 0.25. Solid lines denote particle orbits; dashed and dash-dotted lines respectively denote $\theta = 0$ and $\dot{\phi} = 0$. The arrows on the latter curves mark the sense of admissible transitions between adjacent domains.

(as the one originating at E) trajectories. One still needs to determine whether these trajectories are closed or spiral. In the cases $\bar{\phi} = 0, \frac{1}{2}\pi$ only periodic solutions are possible: when $\bar{\phi} = \frac{1}{2}\pi$, $\mathrm{d}\theta/\mathrm{d}\phi$ is an odd function of ϕ, and therefore θ is an even function of ϕ. This symmetry relative to the x-axis leads to the conclusion that an orbit which intersects the x-axis twice is necessarily closed. Since in this case the eigenvalues of $\nabla_{\boldsymbol{e}} \dot{\boldsymbol{e}}|_{\boldsymbol{e}_c}$ are purely imaginary (cf. (4.8) *et seq.*), particle trajectories cannot approach this critical point monotonically. It is thereby established that the equilibrium point $\boldsymbol{e}_c$ is a centre and all the orbits must be closed. When $\bar{\phi} = 0$, a similar reasoning based on the symmetry relative to the y-axis in conjunction with (4.8) leads to the same conclusion. When $\bar{\phi} \neq 0, \frac{1}{2}\pi$, it has been established in the preceding subsection (see (4.8) *et seq.*) that any equilibrium point off the equator is either a spiral point or a node.

The foregoing discussion is illustrated in figure 3(*b*) by the spiral particle trajectories originating at E and near A (obtained by numerical integration of (4.1)). According to (4.8) in conjunction with (4.4*a*), the critical point A is an unstable spiral point (for $\bar{\phi} = \frac{1}{4}\pi$) and indeed both orbits move away from A and eventually converge to a limit cycle along the equation $\theta = \frac{1}{2}\pi$ (which again is in agreement with the Poincaré–Bendixon theorem).

The motion of slightly deformed spheres

In the context of the latter example it is enlightening to consider the asymptotic limit of slightly deformed spheres ($B \approx o(1)$) in the presence of a sufficiently weak ($\lambda < 1/2$) external field. In these circumstances a dipolar sphere undergoes a periodic rotary motion during which the vector $\boldsymbol{e}$ attached to the dipole axis traverses one of an infinite family of closed circular orbits on the surface of the unit sphere (the specific trajectory being selected according to the orientation of the dipole axis at some initial instant of time).

Similarly to Hinch & Leal (1972*b*), we select here a right-handed space-fixed Cartesian frame of reference (x_1, x_2, x_3) such that the x_1-axis is parallel to the undisturbed fluid vorticity vector and the direction of x_3 coincides with that of the external field (see figure 4). The rotary motion of the particle is parameterized in terms of α, the polar angle of the permanently fixed axis about which the dipolar sphere rotates (the orbit parameter), together with β, the phase angle measured counter-clockwise along the circular trajectory ($\beta = 0$ corresponding to the orbit point where $\boldsymbol{e}$ is closest to the x_1-axis). Expressing the components of $\boldsymbol{e}$ and $\dot{\boldsymbol{e}}$ in the frame (x_1, x_2, x_3), it is established† from the equation of motion (2.1) that

$$\dot{\alpha} = \frac{1}{2}\frac{B\sin\alpha}{e_1}\{[e_1\cos\alpha - (e_1^2 + 2e_3^2)(e_1\cos\alpha - e_2\sin\alpha)]\sin 2\bar{\phi} + e_3[2e_1e_2\cos\alpha + (1-2e_2^2)\sin\alpha]\cos 2\bar{\phi}\}, \quad (4.12a)$$

and

$$\dot{\beta} \approx \tfrac{1}{2}\cos\alpha + A\cos\beta + O(B), \quad (4.12b)$$

in which $e_i (i = 1, 2, 3)$ denote the respective components of $\boldsymbol{e}$ in the (x_1, x_2, x_3) frame of reference and $A \overset{\text{def}}{=} [\lambda^2 - (1/4)\sin^2\alpha]^{1/2}$. We thus anticipate that for $B \approx o(1)$ the solution is approximately the periodic orbit of a dipolar sphere slowly modified by particle drift across orbits. This suggests the multiple-timescale expansion

$$\alpha \approx \alpha_0(\tau, \tau_1) + B\alpha_1(\tau, \tau_1) + O(B^2), \quad (4.13a)$$

$$\beta \approx \beta_0(\tau, \tau_1) + B\beta_1(\tau, \tau_1) + O(B^2), \quad (4.13b)$$

† Cf. the footnote pertaining to (3.2).

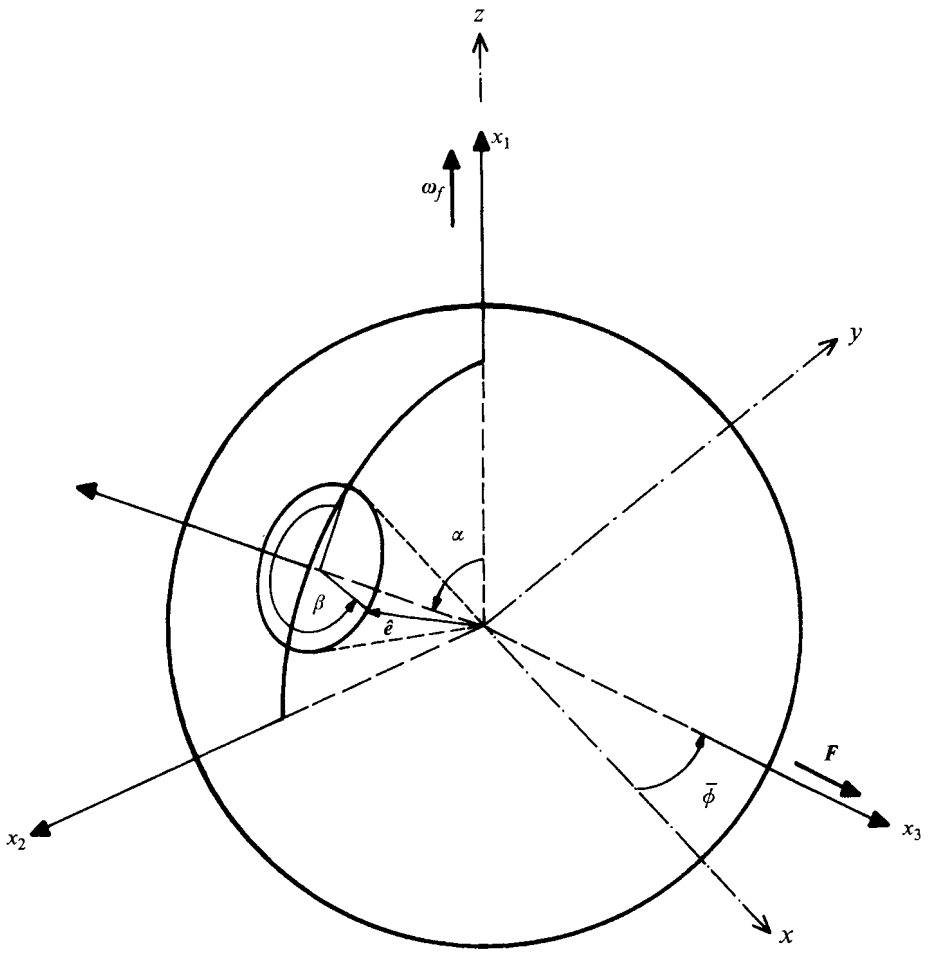

FIGURE 4. Definition of orbit coordinates for slightly deformed dipolar spheres.

where
$$\tau_1 = B\tau \tag{4.14}$$
is the 'slow' time variable. Substitution into (4.12*a*) of the expansions (4.13) yields at the $O(1)$ leading order
$$\partial\alpha_0/\partial\tau = 0 \tag{4.15a}$$
and
$$\partial\beta_0/\partial\tau = \tfrac{1}{2}\cos\alpha_0 + A\cos\beta_0. \tag{4.15b}$$
The former of these equations is readily integrated to obtain $\alpha_0 = \alpha_0(\tau_1)$. The latter equation is identical to the equation governing the motion of a dipolar sphere (cf. Brenner 1970; Hinch & Leal 1972*b*). For $\lambda < 1/2$ it yields periodic solutions in τ.

Our main goal is to determine the variation of α_0 on the slow timescale. Writing the $O(B)$ balance of (4.12*a*) and imposing the requirement that α_1 be periodic in τ leads after some manipulation to
$$\frac{\partial\alpha_0}{\partial\tau_1} = \tfrac{1}{2}\sin 2\bar{\phi}\sin\alpha_0\frac{(1-4\lambda^2)^{1/2}}{4\lambda^2}\left[1+\cos^2\alpha_0 - 2\frac{1-2\lambda^2}{(1-4\lambda^2)^{1/2}}\cos\alpha_0\right]. \tag{4.16}$$
While (4.16) could be integrated formally to yield $\tau_1 = \tau_1(\alpha_0)$, it suffices for our

present purpose to examine the sign of $\partial\alpha_0/\partial\tau_1$. Throughout the allowable interval $(1-4\lambda^2)^{1/2} \leqslant \cos\alpha \leqslant 1$, the expression in square brackets on the right-hand side of (4.16) is negative. Consequently, the sign of $\partial\alpha_0/\partial\tau_1$ is determined by $\bar{\phi}$, the direction in the plane of the flow of the external field. Thus, for $0 < \bar{\phi} < \frac{1}{2}\pi$, $\partial\alpha_0/\partial\tau_1 < 0$ and accordingly the particle drifts across the circular orbits in a spiral trajectory approaching the equator. Alternatively, when $\frac{1}{2}\pi < \bar{\phi} < \pi$, $\partial\alpha_0/\partial\tau_1 > 0$ and the particle spirals towards the critical point. These results support the general statements (cf. (4.8) *et seq.*) regarding the stability of the critical points. Finally, when $\bar{\phi} = \frac{1}{2}\pi$, $\partial\alpha_0/\partial\tau_1 = 0$ and thus the departure from the closed orbit is, within the present calculation, a higher-order effect. This latter result is the asymptotic counterpart of the more general result established above, namely that, even for $|B|$ which is not necessarily small, particle orbits are periodic in these cases.

The intermediate regime

Some interesting modes of behaviour appear in the intermediate interval of λ values for which the ellipse $\dot{\phi} = 0$ cross the equator $\theta = \frac{1}{2}\pi$ at four points (cf. §4.2). These are illustrated in figure 5 for $\lambda = 0.75$ and $B = 0.8$.

In figure 5(*a*) $\bar{\phi} = 88°$. The critical points on the equator are: A – a stable node; B and C – saddle points; and D – an unstable node. Additionally, there exists the unstable spiral point E within the unit circle. (The latter represents the projection on the (x, y)-plane of a pair of critical points symmetrically placed on the upper and lower hemispheres, respectively.) The dotted lines show the separatrices (entire trajectories) respectively joining the saddle point C to the stable node A and the spiral point E to the saddle B. Also shown are representative (positive) semi-trajectories starting at F and G.

When $\bar{\phi}$ is replaced by $\pi - \bar{\phi}$ then, according to (2.8*d*), the appropriate picture is obtained via a reflection with respect to the horizontal x-axis accompanied by a reversal of the sense of the motion along the various orbits. Thus for $\bar{\phi} = 92°$, D′, the reflection of D, is a stable node, the images C′ and B′ are saddle points, A′ is an unstable node, and E′ is a stable spiral point.

Despite the geometric similarity of the two pictures, there is an essential difference between particle motions in the two cases. For $\bar{\phi} = 88°$ all particles, irrespective of their initial orientations, converge for sufficiently long times to the stable equilibrium orientation at A. On the other hand, when $\bar{\phi} = 92°$ the separatrix from the unstable node A′ to the saddle point C′ divides the upper hemisphere into two domains of attraction. Only particles whose initial orientations are to the right of the entire trajectory A′C′ will eventually reach the stable node D′. The rest of the particles will converge to the stable spiral point at E′ (or else to its image on the lower hemisphere). For $\bar{\phi} = 92°$ and larger values of $0.859 < \lambda < 0.901$ (cf. figure 2*b*) a pair of stable equilibrium orientations appear simultaneously as stable nodes on the equator. (In general, the latter phenomena exist for some interval of external-field directions $\bar{\phi} > 90°$. The extent of this interval increases with $|B|$, e.g. for $B = 0.8$, $90° < \bar{\phi} < \sim 105°$.)

Also interesting is the symmetric case $\bar{\phi} = \frac{1}{2}\pi$ presented in figure 5(*b*). In this case the dotted line joining the saddle points C and B divides the upper half of orientation space into two domains of attraction in which the respective modes of particle motion are qualitatively different. Particles originally to the right of BC will converge to the stable node A, whereas the domain to the left of BC is spanned by a family of periodic orbits encircling the centre at E. Similarly to any system having a separatrix connecting saddle points, the present configuration is structurally unstable. Indeed, $\bar{\phi} = \frac{1}{2}\pi$ is a bifurcation value where the topology of the system switches from an unstable spiral

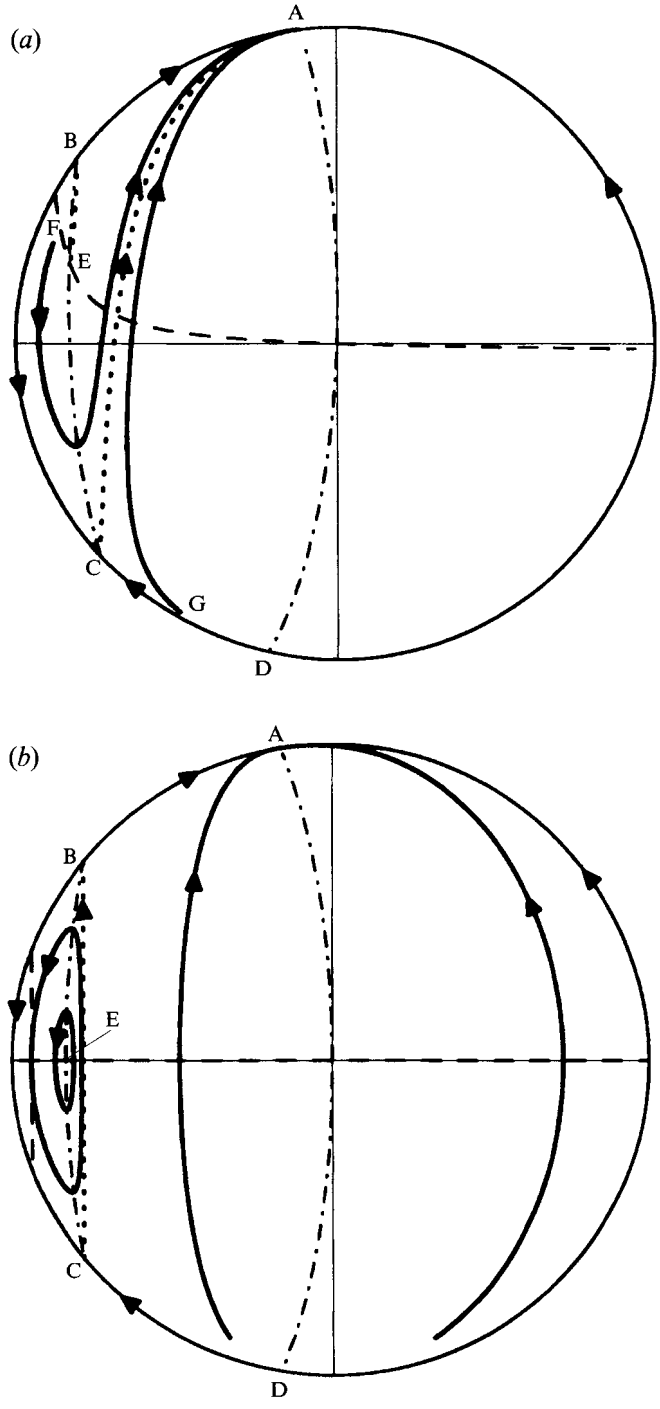

FIGURE 5. Projections on the plane of shear of particle trajectories in the intermediate regime for $B = 0.8$, $\lambda = 0.75$, and external field acting in the plane of shear in the direction (*a*) $\bar{\phi} = 88°$ and (*b*) 90°. Entire particle trajectories joining critical points (separatrices) are presented by dotted lines; other orbits by solid lines; dashed and dash-dotted lines respectively denote $\dot{\theta} = 0$ and $\dot{\phi} = 0$.

point surrounded by a stable limit cycle to a configuration of a stable spiral point together with an unstable limit cycle.

5. External field acting in an arbitrary direction $\bar{\theta} \neq 0, \frac{1}{2}\pi$

5.1. *The limit of weak* ($\lambda \ll 1$) *external field*

Assuming that $1-|B| \approx O(1)$, one infers from (2.7*a*) that $\theta_c \approx O(\lambda)$ (and, of course, an additional point near the pole $\theta = \pi$). Substitution into (4.5) while utilizing (2.7) yields the eigenvalues of $\nabla_e \dot{e}|_{e_c}$

$$S_j = \pm\tfrac{1}{2}\mathrm{i}\,(1-B^2)^{1/2} - \lambda\cos\bar{\theta} + O(\lambda^2) \quad (j = 1, 2). \tag{5.1}$$

Thus, for $\cos\bar{\theta} \approx O(1)$, the critical point on the upper (lower) hemisphere is a stable (unstable) spiral point irrespective of $\bar{\phi}$.

In the present limit, we anticipate that the particle's motion be nearly periodic along Jeffery orbits and that small departures from these closed contours resulting from the action of the external field will accumulate and manifest themselves in the long-time limit in the form of a slow drift of the particle across these orbits. Accordingly, we assume here the multiple-scale expansions

$$\theta = \theta_0(\tau, \tau_1) + \lambda\theta_1(\tau, \tau_1) + O(\lambda^2) \tag{5.2a}$$

and

$$\phi = \phi_0(\tau, \tau_1) + \lambda\phi_1(\tau, \tau_1) + O(\lambda^2) \tag{5.2b}$$

in which

$$\tau_1 = \lambda(\tau - \tau_0) \tag{5.3}$$

denotes the slow time variable and the constant τ_0 is some initial time. When the above are substituted into (2.7), one obtains at the $O(1)$ leading-order balance

$$\partial\phi_0/\partial\tau = \tfrac{1}{2}(1 + B\cos 2\phi_0) \tag{5.4a}$$

and

$$\partial\theta_0/\partial\tau = \tfrac{1}{4}B\sin 2\theta_0 \sin 2\phi_0, \tag{5.4b}$$

which system of equations is integrated (Jeffery 1922) to yield

$$\tan\phi_0 = R\tan\left[2\pi\frac{\tau - \tilde{\tau}(\tau_1)}{T}\right] \tag{5.5a}$$

and

$$\tan\theta_0 = C(\tau_1)\left\{\cos^2\left[2\pi\frac{\tau-\tilde{\tau}(\tau_1)}{T}\right] + R^2\sin^2\left[2\pi\frac{\tau-\tilde{\tau}(\tau_1)}{T}\right]\right\}^{1/2}. \tag{5.5b}$$

Thus, on the fast timescale, the rotary motion is indeed periodic, possessing the same period, namely $T = 2\pi(R + R^{-1})$ along all Jeffery orbits. The difference between (5.5) and the rotary motion of an axisymmetric particle in the absence of an external field appears in the functional dependence on τ_1, the slow time variable, of $\tilde{\tau}(\tau_1)$, the phase shift, and $C(\tau_1)$, the orbit parameter. The latter dependence represents the possible slow drift of the particle across orbits. Eliminating the secular terms in the system of equations governing the respective first-order correction terms, θ_1, and ϕ_1, one obtains†

$$\mathrm{d}\tilde{\tau}/d\tau_1 = 0 \tag{5.6a}$$

and

$$\frac{\mathrm{d}C}{\mathrm{d}\tau_1} = -\frac{2}{\pi}\cos\bar{\theta}|C|(1 + C^2R^2)^{1/2}\,E\left(\frac{C^2(R^2-1)}{1+C^2R^2}\right), \tag{5.6b}$$

† Cf. the footnote pertaining to (3.2).

where $E(\,)$ denotes the complete elliptic integral of the second kind of the argument in braces. Equation (5.6*a*) shows that there is no phase shift at the leading order. From (5.6*b*) we conclude that for all $0 < \bar{\theta} < \frac{1}{2}\pi$ ($\cos\bar{\theta} \approx O(1)$) and $C \neq 0$ (i.e. $\theta \neq 0, \pi$) $\mathrm{d}C/\mathrm{d}\tau_1 < 0$, i.e. on the slow timescale, the particle drifts across Jeffery orbits spiralling towards the pole $\theta = 0$. This accords with the above statement (cf. (5.1) *et seq.*) that the critical point on the upper hemisphere is a stable spiral point.

It is interesting to express the latter result in terms of the total flux induced by the external field across Jeffery orbits. This flux is given by

$$Q = \lambda \int_c \mathrm{d}s\, \hat{\boldsymbol{n}} \cdot f(C, \tau)\, \dot{\boldsymbol{e}}, \tag{5.7}$$

where, by definition, only that part of $\dot{\boldsymbol{e}}$ associated with the external field contributes to the integrand. Substituting for $f(C, \tau)$, the weight function appropriate to rotary motion along Jeffery orbits (cf. Leal & Hinch 1971) and performing the requisite integration one obtains by comparison with (5.6*b*) that

$$\frac{\mathrm{d}C}{\mathrm{d}\tau_1} = \frac{Q}{2\pi\lambda} \tag{5.8}$$

when $\bar{\theta} = \frac{1}{2}\pi$, $Q = 0$. Particle motion across Jeffery orbits (as seen, for instance, in the spiral trajectories of figure 3*b*) is then a higher-order effect in λ, depending upon local deviations of the particle from Jeffery orbits. Accumulation of these deviations due to stability or instability of the critical point results in 'tightly' winding (for $\lambda \ll 1$) spiral trajectories.

5.2. *Effects of external field intensity and direction*

Under the action of a strong ($\lambda \gg 1$) external field, the critical point on the upper hemisphere is located within an $O(\lambda^{-1})$ neighbourhood of $(\bar{\theta}, \bar{\phi})$. (There is, of course, another equilibrium point located near $(\pi - \bar{\theta}, \bar{\phi} + \pi)$ on the lower hemisphere.) Making use of (2.7) and (4.5) we obtain the eigenvalues of $\nabla_{\boldsymbol{e}} \dot{\boldsymbol{e}}|_{\boldsymbol{e}_c}$

$$S_j = -\lambda + s_j + O(\lambda^{-1}) \quad (j = 1, 2), \tag{5.9}$$

where $s_j (j = 1, 2)$ satisfy a quadratic equation possessing a pair of real solutions provided that

$$\sin^2\bar{\theta} > 2\frac{(1-B^2)^{1/2}[(1-B^2\cos^2 2\bar{\phi})^{1/2} - (1-B^2)^{1/2}]}{B^2 \sin^2 2\bar{\phi}}, \tag{5.10}$$

i.e. if $\bar{\theta}$ is sufficiently large, $\boldsymbol{e}_c$ is a stable node. (Thus, since the latter inequality is satisfied identically (for all B and $\bar{\phi}$) when $\bar{\theta} = \frac{1}{2}\pi$, the critical point near $\bar{\phi}$ on the equator is always a stable node in agreement with the results of the preceding section.) When (5.10) is not satisfied, it is a stable spiral point (see figure 6). Finally, when $|B| \to 1$, $\boldsymbol{e}_c$ is a stable node for all $\bar{\theta}$ because, for rod-like ($R \to \infty$) or disk-like ($R \to 0$) particles, the rotary motion induced by the shear flow (2.4) is no longer periodic. (Evidently, the other equilibrium point is, respectively, an unstable node or spiral point.)

We have seen that (cf. (3.2)), in the particular case of a strong external field acting perpendicularly to the plane of the shear flow ($\bar{\theta} = 0$), the particle approaches the stable equilibrium orientation exponentially rapidly. The above results indicate that this behaviour is a general attribute of the strong-field limit. We thus suggest the following summary of the effects upon the motion of the particle of the field intensity

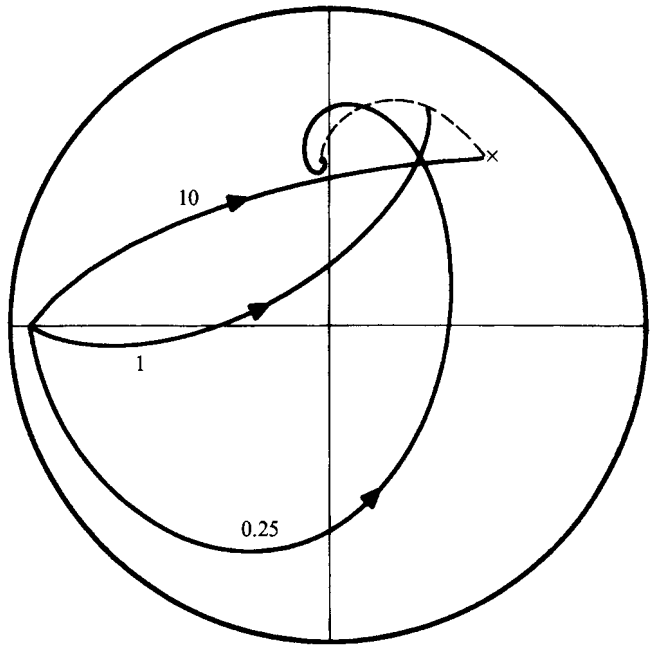

FIGURE 6. Effect of external-field intensity on particle trajectories for $B = 0.5$; $\bar{\theta} = \frac{1}{4}\pi$, $\bar{\phi} = \frac{1}{4}\pi$ and the indicated values of λ. The dashed curve marks the variation with λ of the (stable) equilibrium orientation.

of an arbitrarily oriented external field (assuming for the time being that $\cos\bar{\theta} \approx O(1)$, i.e. the external field is not nearly coplanar with the plane of the flow). With increasing λ the (stable) critical point gradually moves from the vicinity of the pole $\theta = 0$ towards the direction $\bar{\boldsymbol{e}} = (\bar{\theta}, \bar{\phi})$, of the external field. For a sufficiently strong field this critical point can change from a stable spiral point to a stable node, provided that (5.10) is satisfied. Furthermore, the particle, which for $\lambda \ll 1$ slowly approaches the equilibrium point along a winding spiral trajectory, converges to $\boldsymbol{e}_c$ more and more rapidly with increasing λ. The foregoing description is illustrated in figure 6 depicting the projections on the plane of shear of particle trajectories starting at $\theta = \frac{7}{18}\pi$, $\phi = \pi$ for $B = 0.5$, $\theta = \frac{1}{4}\pi$, $\phi = \frac{1}{4}\pi$, and $\lambda = 0.25$, 1, 10. The broken line marks the motion of the stable equilibrium point with increasing λ. Although it is hardly discernible in the figure, the critical point remains a (stable) spiral point, as can be verified from (5.10).

Finally, we consider the variation of particle motion with the direction of the external field, namely with $\cos\bar{\theta}$ increasing from zero to $O(1)$, for sufficiently small values of λ (such that the corresponding critical points for $\bar{\theta} = \frac{1}{2}\pi$ lie off the equator). When $\cos\bar{\theta} = \epsilon \ll 1$, the eigenvalues of $\nabla_{\boldsymbol{e}}\dot{\boldsymbol{e}}|_{\boldsymbol{e}_c}$ thus satisfy the quadratic equation (4.8) with the right-hand side replaced by an $O(\epsilon)$ term. Thus, as long as $\cos\theta_c \approx O(1)$, these eigenvalues are complex and $\boldsymbol{e}_c$ is accordingly a spiral point or a centre.

With increasing $\cos\bar{\theta}$ the particle trajectories and critical points become increasingly asymmetric (with respect to the equator). Thus, if for $\bar{\theta} = \frac{1}{2}\pi$ both critical points are unstable spiral points, then with increasing $\cos\bar{\theta}$ the critical point on the upper hemispherical surface becomes less unstable and the one on the lower hemisphere becomes more unstable. At the same time, the limit cycle which, for $\bar{\theta} = \frac{1}{2}\pi$, coincides with the equator shifts closer to and eventually collapses onto the critical point on the upper hemisphere, at which instant the latter transforms into a stable spiral point (a

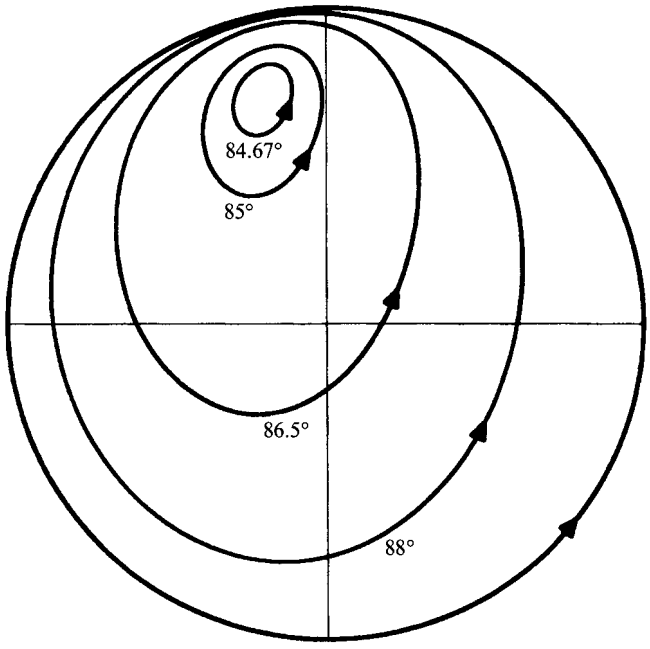

FIGURE 7. Effect of external-field direction on particle trajectories for $B = 0.5$, $\bar{\phi} = \frac{1}{4}\pi$, and $\lambda = 0.25$. The solid lines show the respective limit cycles corresponding to the indicated values of $\bar{\theta}$.

Hopf bifurcation). This sequence of events is described in figure 7 which shows the respective (projections of the) limit cycles for $\lambda = 0.25$, $B = 0.5$, $\bar{\phi} = \frac{1}{4}\pi$ and $\bar{\theta} = 88°$, 86.5°, 85°, and 84.67°. (It is interesting to mention that, for these values of λ and B, one finds via extrapolation of the linear $O(\epsilon)$ expression for the real part of the eigenvalues of $\nabla_e \dot{e}|_{e_c}$ that the latter changes its sign at $\epsilon \approx 0.105$, i.e. $\bar{\theta} \approx 84°$ corresponding to the above-mentioned transformation in the nature of the critical point.)

If both critical points are initially (for $\bar{\theta} = \frac{1}{2}\pi$) stable spiral points then, with increasing $\cos\bar{\theta}$, the stability of the point on the upper hemisphere increases while that of the other one decreases. Here, the (unstable) limit cycle will gradually shrink towards the less stable equilibrium point on the lower hemisphere, eventually collapsing onto this point, at which instant the latter changes into an unstable spiral point.

6. Concluding remarks

The bulk properties of the suspension (which will be studied separately in a forthcoming contribution) are essentially determined (Batchelor 1970; Brenner 1972) by the orientational distribution of the particles which, in turn, depends upon the long-time behaviour of the rotary motion of the particles. By the Poincaré–Bendixon theorem, this behaviour may consist of periodic motion along one member of a family of closed orbits (in which case the particles retain dependence upon their respective initial orientations) or else the particles may converge to either a limit cycle or a stable equilibrium orientation.

For comparison we mention here the results of Hall & Busenberg (1969) concerning the motion of a dipolar sphere in which case only two modes of motion exist: for a sufficiently weak ($\lambda < \frac{1}{2}$) external field acting in the plane of the undisturbed shear flow

($\bar{\theta} = \frac{1}{2}\pi$), the particle rotates along one of an infinite family of circular orbits; in all other cases (i.e. whenever $\lambda \geqslant \frac{1}{2}$ or $\bar{\theta} \neq \frac{1}{2}\pi$), the particle converges to a stable equilibrium orientation.

The present results are both quantitatively and qualitatively different. For $\bar{\theta} = \frac{1}{2}\pi$ and sufficiently small values of λ, the resulting motion depends upon $\bar{\phi}$, the azimuthal direction of the external field in the plane of shear. Thus, depending on whether $0 < \bar{\phi} < \frac{1}{2}\pi$ or $\frac{1}{2}\pi < \bar{\phi} < \pi$, the particle respectively approaches a limit cycle on the equator ($\theta = \frac{1}{2}\pi$) or a stable equilibrium orientation, whereas for $\bar{\phi} = 0, \frac{1}{2}\pi$ it continues to move along one of a family of closed orbits. For sufficiently large values of λ, the particles converge to a stationary stable orientation. The transition between the respective 'small' and 'large' values of λ defines in the present problem a finite intermediate domain whose extent depends on both particle shape (represented by B) and the direction $\bar{\phi}$. In this intermediate domain more than one stable equilibrium orientation or different modes of behaviour may simultaneously coexist. An example of the latter situation is presented in figure 5(*b*) where particles originally in a certain part of orientation space approach the stable node whereas the rest of orientation space is spanned by a family of closed orbits.

When the external field does not act in the plane shear and $\cos\bar{\theta} \approx O(1)$, particles invariably approach the stable equilibrium orientation (irrespective of the value of λ and B). However, contrary to the corresponding result for dipolar spheres, the transition between the cases $\cos\bar{\theta} = 0$ and $\cos\bar{\theta} \approx O(1)$ is gradual. Thus figure 7 shows limit cycles for small but non-zero values of $\cos\bar{\theta}$.

This research was supported by the Fund for the Promotion of Research at the Technion.

REFERENCES

BATCHELOR, G. K. 1970 The stress system in a suspension of force-free particles. *J. Fluid Mech.* **41**, 545–570.

BRENNER, H. 1970 Rheology of two-phase systems. *Ann. Rev. Fluid Mech.* **2**, 137–176.

BRENNER, H. 1972 Suspension rheology in the presence of rotary Brownian motion and external couples: elongational flow of dilute suspensions. *Chem. Engng Sci.* **27**, 1069–1107.

BRENNER, H. 1974 Rheology of a dilute suspension of axisymmetric Brownian particles. *Int J. Multiphase Flow* 1, 195–341.

BRETHERTON, F. P. 1962 The motion of rigid particles in a shear flow at low Reynolds numbers. *J. Fluid Mech.* **14**, 284–304.

HALL, W. F. & BUSENBERG, S. N. 1969 Viscosity of magnetic suspensions. *J. Chem. Phys.* **51**, 137–144.

HINCH, E. J. & LEAL, L. G. 1972*a* The effect of Brownian motion on the rheological properties of a suspension of non-spherical particles. *J. Fluid Mech.* **52**, 683–712.

HINCH, E. J. & LEAL, L. G. 1972*b* Note on the rheology of a dilute suspension of dipolar spheres with weak Brownian couples. *J. Fluid Mech.* **56**, 803–813.

HINCH, E. J. & LEAL, L. G. 1979 Rotation of small non-axisymmetric particles in a simple shear flow. *J. Fluid mech.* **92**, 591–608.

JEFFERY, G. B. 1922 The motion of ellipsoidal particles immersed in a viscous fluid. *Proc. R. Soc. Lond.* A **102**, 161–179.

LEAL, L. G. & HINCH, E. J. 1971 The effect of weak Brownian rotations on particles in shear flow. *J. Fluid Mech.* **46**, 685–703.